

# Soft Matter

Accepted Manuscript



This is an *Accepted Manuscript*, which has been through the Royal Society of Chemistry peer review process and has been accepted for publication.

*Accepted Manuscripts* are published online shortly after acceptance, before technical editing, formatting and proof reading. Using this free service, authors can make their results available to the community, in citable form, before we publish the edited article. We will replace this *Accepted Manuscript* with the edited and formatted *Advance Article* as soon as it is available.

You can find more information about *Accepted Manuscripts* in the [Information for Authors](#).

Please note that technical editing may introduce minor changes to the text and/or graphics, which may alter content. The journal's standard [Terms & Conditions](#) and the [Ethical guidelines](#) still apply. In no event shall the Royal Society of Chemistry be held responsible for any errors or omissions in this *Accepted Manuscript* or any consequences arising from the use of any information it contains.

# Hydrodynamic Interactions slow down Crystallization of Soft Colloids

Dominic Roehm,<sup>a,\*</sup> Stefan Kesselheim,<sup>b</sup> and Axel Arnold<sup>b</sup>

Received Xth XXXXXXXXXXXX 20XX, Accepted Xth XXXXXXXXXXXX 20XX

First published on the web Xth XXXXXXXXXXXX 200X

DOI: 10.1039/b000000x

Colloidal suspensions are often argued to be an ideal model for studying phase transitions such as crystallization, as they have the advantage of tunable interactions and experimentally tractable time and length scales. Because crystallization is assumed to be unaffected by details of particle transport other than the bulk diffusion coefficient, findings are frequently argued to be transferable to pure melts without solvent. In this article, we present molecular dynamics simulations of the crystallization in a suspension of colloids with Yukawa interaction which challenge this assumption. In order to investigate the role of hydrodynamic interactions mediated by the solvent, we model the solvent both implicitly and explicitly, using Langevin dynamics and the fluctuating Lattice Boltzmann method, respectively. Our simulations show a significant reduction of the crystal growth velocity due to hydrodynamic interactions even at moderate hydrodynamic coupling. This slowdown is accompanied by a reduction of the width of the layering region in front of the growing crystal. Thus the dynamics of a colloidal suspension differ strongly from that of a melt, making them less useful as a model for solvent-free melts than previously thought.

## 1 Introduction

Crystallization of metal melts is one of the most important and oldest industrial processes, namely casting. Detailed knowledge of the underlying process is necessary to improve production and to develop new high-tech materials. However, melt temperatures range between several hundred and several thousand degrees Celsius, making it difficult to observe crystallization and nucleation directly in experiments. Therefore these processes are often studied using easier accessible model systems, in particular charged colloids in solution<sup>1–3</sup>, for example polystyrene (PS) or polymethylmethacrylate (PMMA) spheres suspended in water<sup>4–6</sup>. Colloidal particles can be produced with a high degree of monodispersity and with widely tunable interactions. Moreover, colloidal particles can be tracked individually using, e.g., confocal microscopy<sup>7–9</sup>, which gives the equivalent of ‘atomic’ resolution in metal melts. This makes them an ideal model for studying crystallization and nucleation.

In colloidal systems the solvent mediates hydrodynamic interactions (HIs) between the suspended particles. These HIs are different compared to the interactions mediated by the electron gas in metal melts. The influence of HIs on the dynamical properties of colloidal suspensions has been extensively studied in recent years<sup>10,11</sup>. For example, Löwen *et al.*<sup>2,12</sup> showed that the ratio of the long-time to short-time

self-diffusion coefficients has a universal value along the fluid freezing line. Recent studies by Pesche<sup>13</sup> and Nägele<sup>14</sup> of quasi-2D dispersions show that HIs have an impact on the self-diffusion function in these soft-sphere suspensions. However, since nucleation and crystal growth happen on much longer time scales, they are commonly believed to be affected by HIs only through the particle diffusion coefficient<sup>15</sup>, which can be measured conveniently in the bulk liquid. In computer simulations of nucleation, under this assumption hydrodynamic interactions can be neglected to avoid the high computational costs that are incurred by including these. Consequently, only a few studies have so far investigated the influence of HIs on nucleation or crystal growth. In a recent study<sup>16</sup>, it was found that hydrodynamic interactions dramatically speed up the nucleation of hard spheres.

In the following, we will show that HIs do have a remarkable influence on the dynamics of crystal growth in a colloidal suspension with soft interactions as well, however slowing down rather than accelerating the process. We have performed molecular dynamics simulations of the crystallization of colloids with Yukawa interactions near a planar wall, using both Langevin dynamics (LV), which suppresses hydrodynamics, and Lattice Boltzmann (LB) simulations, which includes hydrodynamic interactions. By tracking the position of the crystal front, the speed of crystallization was determined, which we found to be significantly affected by the inclusion of HIs. Even for moderate coupling the speed was reduced by a factor of three. To probe the origin of this effect, the mean-squared displacement (MSD) and distribution functions were calcu-

<sup>a</sup> University of Stuttgart, Allmandring 3, 70569 Stuttgart, Germany, Tel: +49(0)711/685-67705; E-mail: [dominic.roehm@icp.uni-stuttgart.de](mailto:dominic.roehm@icp.uni-stuttgart.de)

<sup>b</sup> University of Stuttgart, Allmandring 3, 70569 Stuttgart, Germany

lated in the vicinity of the crystal front, but the structure in this region seems to be unaffected by hydrodynamic interactions. However, we found the crystal to be preceded by a non-crystalline, but strongly layered region of increased density, and the width of this pre-ordered region decreases with increasing hydrodynamic coupling. The reduced growth speed is thus not an effect of reduced bulk transport, but rather of differences in the local ordering dynamics near the crystal interface.

## 2 Simulation method

To investigate the influence of hydrodynamic interactions on crystal growth, we studied the crystallization of particles interacting via a Yukawa pair potential. We use molecular dynamics (MD) simulations including and excluding HIs by employing a fluctuating lattice Boltzmann method<sup>17</sup> and a Langevin thermostat<sup>18</sup>, respectively. By introducing two parallel confining walls, the nucleation barrier is lowered enough that crystallization happens spontaneously without applying special rare event sampling techniques.

As inter-particle pair potential we used a screened Coulomb interaction potential

$$U(r) = l_B k_B T \frac{Q^2 \exp(-\lambda_D r)}{r}, \quad (1)$$

where  $r$  is the distance between two particles,  $k_B$  denotes the Boltzmann constant,  $T$  the temperature and  $Q$  the valency of the interacting particles. The range of the potential is determined by the Debye-Hückel screening length  $\lambda_D$  and its strength by the Bjerrum length  $l_B$ . The static properties of such a Yukawa system can be characterized by two independent dimensionless parameters<sup>1</sup>

$$\kappa = \frac{r_{ws}}{\lambda_D} \quad \text{and} \quad \Gamma = \frac{Q_1 Q_2}{4\pi\epsilon_0 r_{ws} k_B T} = \frac{Q_1 Q_2 l_B}{r_{ws}}, \quad (2)$$

where  $r_{ws} = (3/(4\pi\rho))^{1/3}$  is the Wigner-Seitz radius of the crystal phase and  $\rho$  the particle density. Phase diagrams of systems with Yukawa interactions have been calculated both by Monte Carlo simulations<sup>19</sup> and MD simulations<sup>1,20</sup>, which consistently found three regimes: a fluid phase and two different solid phases with BCC or FCC structure, respectively. For our simulations, we chose  $\kappa = 3.0$  and  $\Gamma = 1260$ , which is slightly above the transition line between the fluid phase and the solid BCC phase. The walls act on the particles via a Weeks-Chandler-Andersen (WCA) potential modeling a hard sphere repulsion<sup>21</sup>. This corresponds to the hard walls that the solvent experiences and improves numerical stability during equilibration. However, because our measurements are performed at least 10 mean particle distances away from the wall, they are not affected by the wall-particle interaction type.

In the implicit solvent simulations, we use a Langevin thermostat<sup>18</sup> that combines drag and random forces on the particles to establish the correct thermal distribution, but suppresses hydrodynamic interactions. The only tunable parameter is the friction  $\gamma_{LV}$ , which is inversely proportional to the diffusion constant  $D^0 = k_B T / \gamma_{LV}$  of isolated particles.

In order to introduce hydrodynamic interactions, we used the fluctuating lattice Boltzmann method<sup>17,22,23</sup> on a three-dimensional (3D) lattice with 19 velocity densities (D3Q19). We treated the colloidal particles as point particles that are coupled to the LB fluid via a friction term<sup>24</sup> with an adjustable friction constant  $\gamma_{LB}$ . The no-slip boundaries modeling the fluid-wall interaction were realized by the link bounce back rule<sup>25</sup>.

In contrast to other methods of including HIs, such as dissipative particle dynamics<sup>26,27</sup>, the LB method allows us to tune the particle diffusion coefficient largely independently of the viscosity  $\eta$  of the fluid. However, the isolated particle mobility is not simply the inverse of  $\gamma_{LB}$ , but also depends on  $\eta$  and the lattice spacing  $a_{LB}$  of the LB grid due to feedback from the moving fluid<sup>24,28</sup>. In fact, the diffusion constant of an isolated particle reads

$$D^0 = \frac{k_B T}{\gamma_{LB}} + \frac{g}{\eta a_{LB}}, \quad (3)$$

where  $g$  is a numerical factor that depends on the details of the applied coupling method. For the applied first order coupling it equals 0.048<sup>28</sup>.

Identical friction parameters in implicit and explicit solvent simulations thus do not lead to the same diffusion coefficient for isolated particles. In the liquid phase, hydrodynamic interactions will introduce further deviations between the obtained diffusion coefficients. To rule out the possibility that this effect would dominate the crystal growth speed, we matched the magnitude of the self-diffusion constant in the liquid phase between the two simulation methods with a procedure outlined in Sec. 3.

The strength of the hydrodynamic interactions can be quantified by the hydrodynamic radius

$$r_H = \frac{k_B T}{6\pi\eta D^0}, \quad (4)$$

which depends both on the viscosity  $\eta$  of the fluid and on the single particle diffusion coefficient  $D^0$ . The higher  $r_H$ , the stronger hydrodynamic interactions are. We use the same quantity also to express the friction constant used in the LV simulations, where we assume the same viscosity as in the LB case.

In the following, we report energies in multiples of the thermal energy  $k_B T$ , lengths in multiples of  $a = \rho^{-1/3}$  and times in multiples of  $\tau = a\sqrt{k_B T/m_p}$ , where  $\rho$  is the particle number density and  $m_p$  the mass of the colloids.  $\tau$  is the time that an isolated particle needs to diffuse over distance  $a$ .

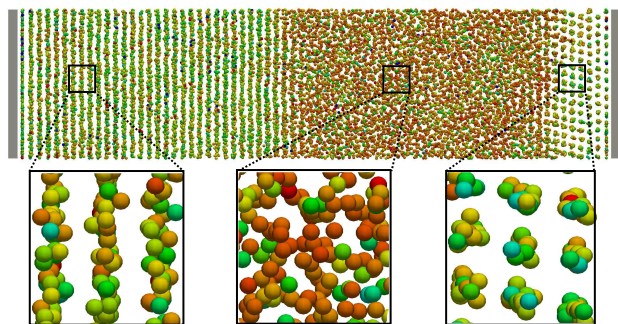


**Fig. 1** Snapshot of the simulation at the end of the run. The color of the particles represents the average Steinhard order parameter  $\bar{q}_6$  (blue-green: solid, yellow-red: liquid). The crystal has grown from the wall layer (gray) into the volume, in this case mainly from the left-hand side. On the right-hand side the crystal structure is the same as on the left, however, the orientation of the crystal is flipped by  $90^\circ$ . The insets show details of the various phases.

If not otherwise stated, the simulations were performed with 16,384 particles in a box of size  $60 \times 14.5 \times 14.5$  confined by two planar walls located at  $x = 0.45$  and  $x = 59.5$ . The equations of motion of the particles with Yukawa interaction were integrated by a Velocity-Verlet integrator<sup>29</sup> with time step  $dt = 0.01$ . In all reported simulations with HIs, we used the same time step also for the LB fluid. The LB fluid grid spacing was chosen to be  $a_{LB} = 0.9$ , the viscosity  $\eta = 0.8$  and the density of the fluid  $\rho_{fl} = 0.75$ . The friction  $\gamma$  varies between 0.5 and 12.5 in case of LB and 0.5 and 6.5 for LV, respectively. All simulations were performed using the MD simulation package *ESPResSo*<sup>30,31</sup> and its GPU-accelerated fluctuating LB implementation<sup>32</sup>.

### 3 Matching the tracer diffusion

The diffusion constant in a liquid phase depends on the hydrodynamic interactions as well as on the particle-particle interactions. In order to set up comparable simulations, we matched the tracer diffusion coefficient, also known as self-diffusion coefficient, in the bulk liquid. This was done by measuring the MSD of tracer particles in a pure bulk system, both with Langevin dynamics and with the Lattice Boltzmann method. These measurements were performed in three-dimensional periodic systems consisting of 16,384 particles in a box of size  $58 \times 14.5 \times 14.5$  without confining walls. This setup ensures that the same finite size effects are present in these simulations as in the production runs. To estimate finite size effects on the tracer diffusion, we also measured it in different cubic boxes of sizes between  $7.5^3$  and  $30^3$  and found that the effects are less than 5%.

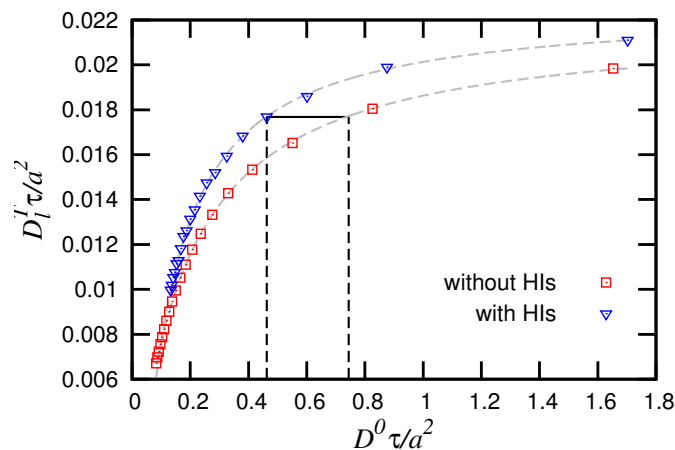


**Fig. 2** The diffusion coefficient of the tracer particles in the bulk  $D_1^T$  as a function of the single particle diffusion coefficients  $D^0$ . (in simulation units). Red squares show results for the system without HIs and the blue triangles for the systems with HI. The gray dashed lines are a guide to eye. The black lines illustrate the matching of the diffusion coefficient. Two different single particle diffusion coefficients  $D^0$  using LV or LB coupling result in the same long-time diffusion coefficient  $D_1^T$ .

Fig. 2 shows the measured long-time diffusion coefficient  $D_1^T$  of tracer particles in the bulk as a function of the single particle diffusion coefficient  $D^0$ . The tracer diffusion coefficients differ significantly between Langevin dynamics and Lattice Boltzmann simulations due to hydrodynamic interactions. In order to match the tracer particle diffusion coefficient  $D_1^T$ , we used different values for the friction coefficient for the LV and the LB coupling and compared only those combinations where the resulting diffusion coefficient in the liquid phase was the same. The black line in Fig. 2 illustrates this matching: in order to obtain for example the same diffusion coefficient  $D_1^T \tau/a^2 = 0.018$ , we have to apply  $\gamma_{LV} = 4.0$  for LV and  $\gamma_{LB} = 7.0$  for LB simulations. In the following, we only report data with matched tracer diffusion coefficients in the bulk, where the given values of  $\gamma$  are always the ones that apply to the LB coupling. The corresponding value of  $\gamma_{LV}$  is smaller and can be calculated from Fig. 2.

### 4 Measuring crystal growth speed

Using the matched tracer diffusion, we investigated the freezing of the undercooled fluid confined between two planar walls. We prepared our system as an undercooled liquid and let the system crystallize. In order to distinguish the liquid and the different solid phases, we used the Steinhardt order

parameter<sup>33</sup>, which for particle  $i$  reads

$$q_l(i) = \sqrt{\frac{4\pi}{2l+1} \sum_{m=-l}^l |q_{lm}(i)|^2}, \quad (5)$$

where

$$q_{lm}(i) = \frac{1}{N_b(i)} \sum_{j=1}^{N_b(i)} Y_{lm}(r_{ij}) \quad (6)$$

is a complex quantity based on the spherical harmonics  $Y_{lm}$  and order  $l$ ,  $N_b(i)$  is the number of nearest neighbors of particle  $i$  and  $r_{ij}$  the distance vector between particles  $i$  and  $j$ .

Depending on the choice of  $l$ , the Steinhardt order parameter is sensitive to various crystal symmetries. In the present case of Yukawa interaction the solid phases are either FCC or BCC crystals, which the  $q_6$  order parameter distinguishes well from a liquid<sup>34</sup>. In order to dampen the thermal fluctuations, we applied an averaging method introduced by Lechner<sup>35</sup>:

$$\bar{q}_l(i) = \sqrt{\frac{4\pi}{2l+1} \sum_{m=-l}^l |\bar{q}_{lm}(i)|^2}, \quad (7)$$

with

$$\bar{q}_{lm}(i) = \frac{1}{\tilde{N}_b(i)} \sum_{k=0}^{\tilde{N}_b(i)} q_{lm}(k), \quad (8)$$

where  $\tilde{N}_b(i)$  is the number of the neighboring particles and the particle  $i$  itself. The literature values<sup>35</sup> are  $\bar{q}_6(\text{BCC}) = 0.408018$ ,  $\bar{q}_6(\text{HCP}) = 0.42181$  and  $\bar{q}_6(\text{LIQ}) = 0.161962$ .

Figure 3 shows the measured  $\bar{q}_6$  of three snapshots taken at different times during a typical simulation run. Note that the points only represent the peaks of  $\bar{q}_6$  profile, which shows strong layering parallel to the wall. Between the peaks the density drops nearly to zero in the crystal, and consequently so does the order parameter. And because we report only the peak values, the  $\bar{q}_6$  in the liquid bulk is larger than the literature average value.

As expected, the crystal starts with a HCP wall layer, followed by a BCC crystal front that grows with time. To evaluate the position of the crystal front, we fitted the  $\bar{q}_6$  peaks to a function of shape

$$-h \left[ \frac{1}{\pi} \arctan \left( \frac{(x-s)}{w} - 0.5 \right) \right] + \bar{q}_{6,\text{bulk}}, \quad (9)$$

where  $x$  is the  $x$ -position in the simulation box,  $h$  is the height difference between bulk  $\bar{q}_6$ , and the BCC  $\bar{q}_6$ ,  $w$  is the width of the liquid-crystal transition region and  $s$  is the position of the crystal front.

Figure 4 shows the evolution of the position of the front as a function of time in the linear regime of two arbitrarily chosen simulation runs. Clearly the slopes are linear over a range of

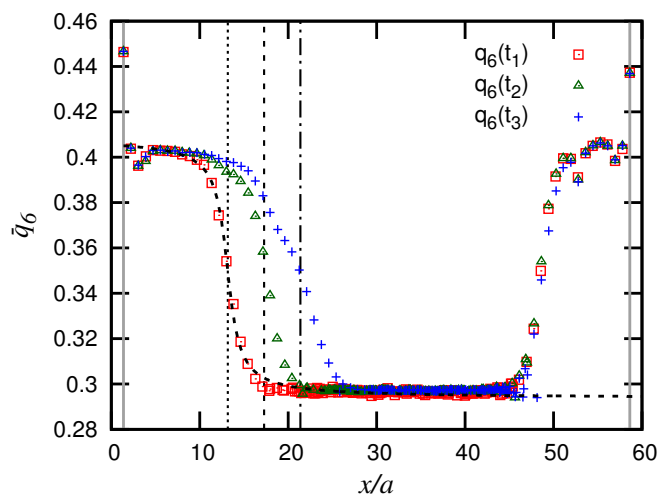


**Fig. 3** This figure shows our fitting procedure for  $s$  (position of the crystal front), from the shape of  $\bar{q}_6$  as a function of  $x$  for different times  $t_1 < t_2 < t_3$ . The symbols represent the peaks of the  $\bar{q}_6$  order parameter. The vertical dashed lines indicate the computed front locations ( $s_1 < s_2 < s_3$ ), while the dashed line through the red data points shows the fit for  $\bar{q}_6$  at time  $t_1$ .

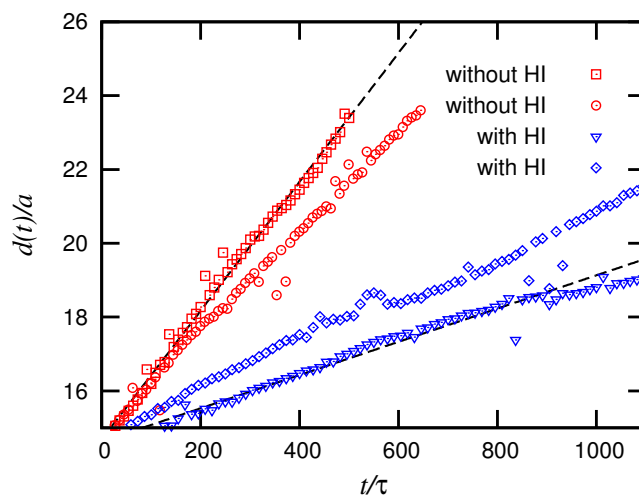


**Fig. 4** Examples of the position of the crystal front as a function of time for four different runs with (blue) and without HI (red) at matched  $D_l^T = 0.012$ . All systems show a linear trend, as illustrated by the black dashed lines. The slope of these lines gives the front growth velocity.

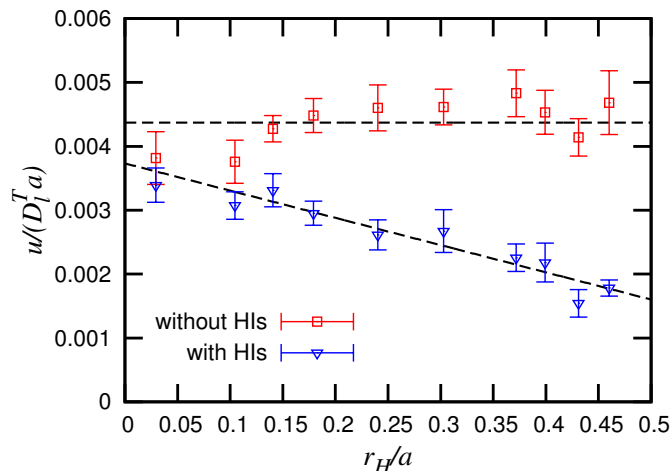


**Fig. 5** Growth velocity  $u$  normalized by the bulk diffusion coefficient  $D_l^T$  as a function of the hydrodynamic radius  $r_H$ . The red squares show the results for simulations without HIs, which are independent of  $r_H$  within error bars. The blue triangles represent the results for simulations with HIs, which show a strong decay of the growth velocity with increasing hydrodynamic radius. The black dashed lines are guidelines to eye.

about 20% of the total box length, but with significantly different slopes depending on whether HI are taken into account or not. Therefore, we can fit the front position to a linear function  $d(t) = u \cdot (t - t_0)$  to determine the growth speed. In order to minimize effects due to the walls, we start only after about 15 crystal layers have grown, and stop when about 40% of the box length are reached to avoid interactions with the crystal possibly growing from the opposite wall.

Figure 5 shows the measured velocities  $u$  as a function of the hydrodynamic radius  $r_H$ , which we varied by changing the friction coefficient  $\gamma$  and applying the matching procedure described above. Every measurement represents the mean growth velocity sampled from 24 independent runs. Using Langevin dynamics, the normalized growth velocity is virtually constant as one would expect, where the rate is proportional to the long-time diffusion coefficient  $D_l^T$ . Using a Lattice Boltzmann fluid, this picture however changes. For very small hydrodynamic radii  $r_H < 0.025$ , the influence of HI is almost negligible as one would expect. But already in case of moderate ratios  $0.1 < r_H < 0.25$ , hydrodynamic interactions reduce the crystal growth velocity significantly, up to a factor of 3 at  $r_H = 0.5$ .

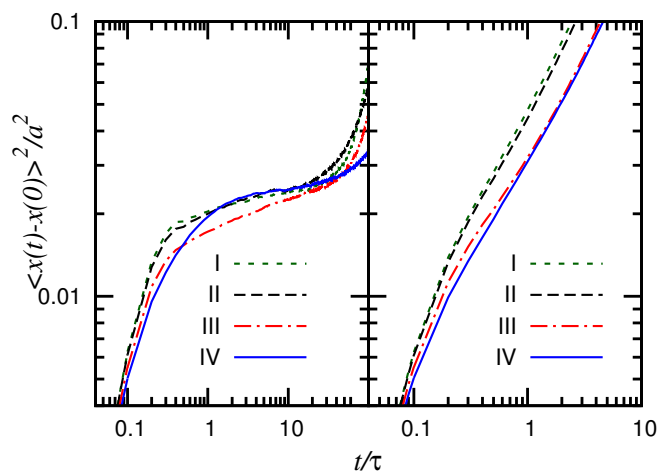


**Fig. 6** Right: MSDs far away from the crystal front in the bulk liquid. The first two cases (I: LV, II: LB) have  $r_H = 0.06$ , cases III (LV) and case IV (LB)  $r_H = 0.44$ . The MSDs with and without hydrodynamic interactions agree well on all time and length scales, reflecting the matched long time diffusion coefficient. Left: MSDs at the crystal front for the same four cases. At  $r_H = 0.06$ , the simulations with and without hydrodynamic interactions mostly coincide. For  $r_H = 0.44$ , however, case III with LV differs notably at intermediate times from case IV with LB, despite the short time behavior being the same for both. At long times, the MSD becomes quadratic due to the material transport across the crystal front.

## 5 Transport to the crystal front

In this section we investigate the transport of particles to the crystal front. To this aim we divided our system along the direction of growth in bins of size  $\Delta x = 2$ , so that there are two layers per bin in the crystal phase. We then determined the bin in which the crystal front is located using the  $\bar{q}_6$  order parameter and averaged the mean square particle displacement (MSD) in the direction of growth in a frame co-moving with the front position. Fig. 6 shows the measured MSD of particles in the fluid far from the crystal as well as right at the front for weak and strong HIs. While the MSDs in the bulk fluid show no significant dependence on the strength of HIs over all length and time scales, the MSDs close to the growing crystal front show a considerable difference in the mobility of the particles at strong HIs. At long time scales, the MSDs are quadratic due to the continuous material transport across the moving crystal front. Hence, their magnitudes directly reflect the different growth speeds observed. However, also on intermediate time scales the particles are significantly more mobile if HIs are strong. The magnitude of this increased mobility cannot be explained by the much slower long-term mass transport. Thus, when including hydrodynamic interactions, mobility is increased on the intermediate regime, but reduced on longer time scales.

## 6 Structure of radial distribution function and extent of pre-ordering region

In order to further study the ordering process, we concentrate on the region in front of the growing crystal. As shown in Fig. 7, there is a notable pre-ordering region in front of the crystal, where the density and layering already correspond to the final crystal structure, but the local order as measured by  $\bar{q}_6$  is still disturbed.

In order to obtain a deeper insight into the ordering process, we analyzed the two dimensional radial distribution function (RDF)  $g(r) = \rho(r)/\langle\rho\rangle$  in slices perpendicular to the growth direction. To that aim we binned our system such that each bin contains a single crystal layer and compute the RDF once deep in the crystal and at the position of the density front as shown in Fig. 8. As expected, the (static) crystal structures are unaffected by hydrodynamic interactions. However, even at the position of the density front, which is between one and three particle layers in front of the actual crystal, the RDFs hardly show any difference to the crystal phase. While RDFs in the fluid phase have only one significant peak and quickly decay to 1, here strong correlations extend over several particle diameters. Thus, the long-range order of the crystal is already well established in the pre-ordering region, independent of the strength of hydrodynamic interactions.

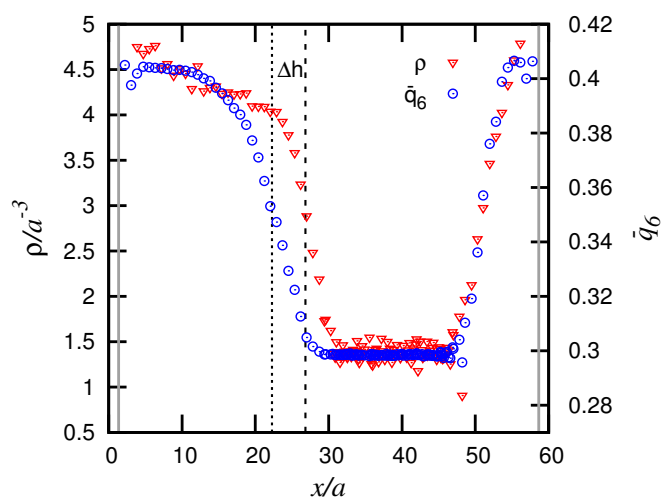


**Fig. 7** Peaks of density ( $\rho$ ) and  $\bar{q}_6$  order parameter during a simulation for a case with strong HIs ( $r_H = 0.44$ ). This (arbitrarily chosen) snapshot illustrates the lag between the density front and the  $\bar{q}_6$  order parameter front. The dashed black lines show the location of the front determined from fitting Eq. (9) for density and  $\bar{q}_6$ , respectively.

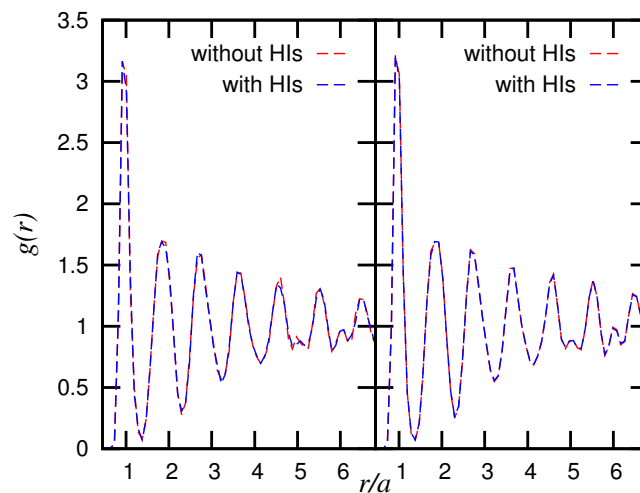


**Fig. 8** Left: radial distribution function (RDF) parallel to the confining walls at the density front with and without HIs at  $r_H = 0.44$ . The density front is located 2.5 after the  $\bar{q}_6$  front for the LV simulations and 1.6 for the LB simulations. Right: RDF deep in the crystal phase for the same parameters. Two features are remarkable: first, the long-range order is already established far in front of the  $\bar{q}_6$  front. Second, the long-range order does not seem to be affected by HIs.

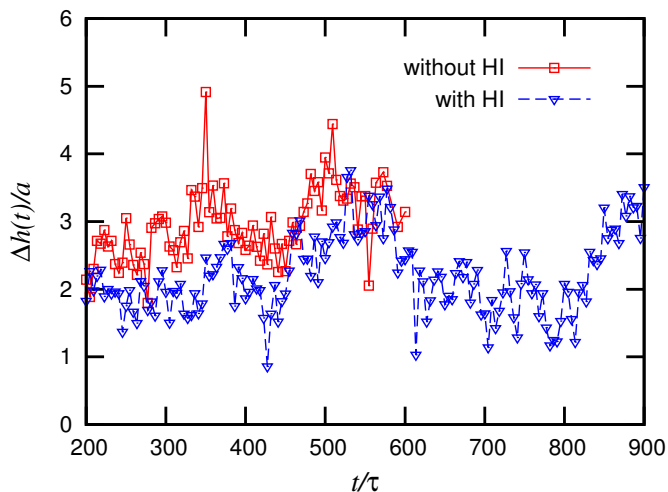


**Fig. 9** The width of the pre-ordering region  $\Delta h(t)$  over the time  $t/\tau$ , exemplary shown for two cases of Fig. 4 in the regime of linear growth. The red curve shows the results in case of no HIs, while the blue case is with HIs. The width  $\Delta h(t)$  is virtually constant and clearly reduced in case of mediate HIs.

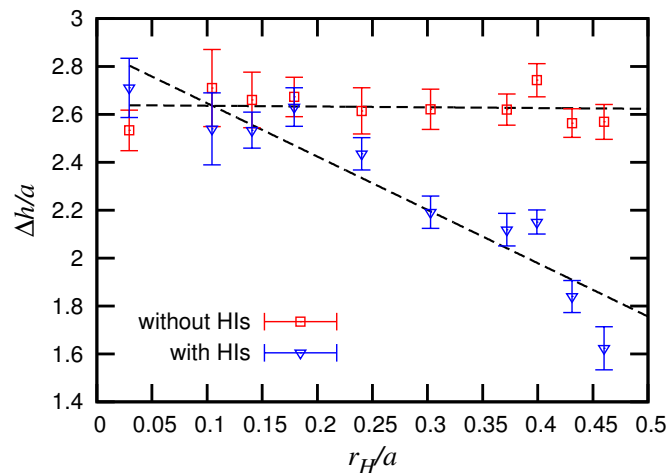


**Fig. 10** The difference  $\Delta h$  between the position of the front detected by the density profile and by the  $\bar{q}_6$  order parameter. While  $\Delta h$  is virtually constant in the absence of HIs, it decreases practically linearly with increasing  $r_H$  if HIs are taken into account. The dashed lines are guides to the eye highlighting the respective constant and linear trends.

However, Fig. 8 hides one remarkable difference. The  $\bar{q}_6$  and density fronts grow virtually equally fast as shown in Figure 9, so that we can define and measure the width  $\Delta h$  of the pre-ordering region. Figure 10 shows that this width decreases with the strength of the hydrodynamic interactions if hydrodynamic interactions are taken into account, while it is constant with implicit solvent. Only at very low hydrodynamic radii, LV and LB simulations lead to the same width. The decrease seems to follow a linear trend similar to the decrease of the crystal growth speed, compare Fig. 5. This shows two things: first, HI seem to hinder the pre-ordering, so that the local arrangement can catch up, while the overall growth is slower. However, as we have shown before, long time transport properties are not responsible for this slower pre-ordering, but rather processes on intermediate time scales. Second, and more importantly, this HI dependent width of the pre-ordering region shows that the system is out of equilibrium, because otherwise the width would not be affected by the underlying dynamics. The fact that the Langevin simulations do not show this behavior underlines that this is not just a bulk transport effect. Thus, the mechanism of crystal growth in colloidal suspensions cannot be fully described as purely diffusive process, where all other degrees of freedom relax much faster than the particles order at the crystal surface.

## 7 Conclusions

We have performed molecular dynamics simulations of the crystallization of particles with Yukawa interaction from a planar wall, modeling the solvent either implicitly by Langevin dynamics or explicitly using a Lattice Boltzmann fluid. Using the implicit solvent, both the crystal growth speed and the width of the pre-ordering region are independent of the friction coefficient. However, using the Lattice Boltzmann fluid we observe that hydrodynamic interactions slow down the crystallization notably even for moderate hydrodynamic radii. This slow down is accompanied by narrowing of the pre-ordering region. Thus, the attachment of particles to a growing crystal is not a purely diffusive process as often assumed.

Our findings are not a specific feature of soft particles or the LB method. For hard spheres embedded in a multi-particle collision fluid, it has recently been shown that hydrodynamic interactions *speed up* nucleation<sup>16</sup>. This might seem surprising at first, but our studies indicate that the main effects are on the length and time scales where the different inter-particle potentials come into play. Unlike soft particles, hard spheres cannot overlap and thus probe longer length scales during attachment.

Since hydrodynamic interactions are omnipresent in suspensions of charged colloids, crystallization and nucleation in these systems cannot be described well as purely diffusive processes. Thus, the often drawn analogy between metal melts and colloidal suspensions should be taken with a sizable

grain of salt. On the other hand, colloidal suspensions can offer valuable input to the development of an out-of-equilibrium theory of nucleation and crystal growth.

## 8 Acknowledgements

We thank J. de Graaf for fruitful discussions and acknowledge financial support from the German Science Foundation (DFG) through SFB716 and the cluster of excellence SimTech.

## References

- 1 S. Hamaguchi, R. Farouki and D. Dubin, *The Journal of chemical physics*, 1996, **105**, 7641.
- 2 H. Löwen, *Physical Review E*, 1996, **53**, 29–32.
- 3 H. Löwen, *Physica A*, 1997, **235**, 129–141.
- 4 R. Klein and P. Meakin, *Nature*, 1989, **339**, 360–362.
- 5 D. Petsev and N. Denkov, *Journal of Colloid and Interface Science*, 1992, **149**, 329–344.
- 6 A. Engelbrecht, R. Meneses and H. Schöpe, *Soft Matter*, 2011, **7**, 5685–5690.
- 7 A. Imhof, A. Van Blaaderen, G. Maret, J. Mellema and J. Dhont, *The Journal of chemical physics*, 1994, **100**, 2170–2181.
- 8 M. E. Leunissen, C. G. Christova, A. P. Hynninen, C. P. Royall, A. I. Campbell, A. Imhof, M. Dijkstra, R. van Roij and A. van Blaaderen, *Nature*, 2005, **437**, 235–240.
- 9 E. R. Weeks, J. C. Crocker, A. C. Levitt, A. Schofield and D. A. Weitz, *Science*, 2000, **287**, 627–631.
- 10 G. Nägele, *Physics Reports*, 1996, **272**, 215–372.
- 11 J. T. Padding and A. A. Louis, *Physical Review E: Statistical, Nonlinear, and Soft Matter Physics*, 2006, **74**, 031402.
- 12 H. Löwen, T. Palberg and R. Simon, *Physical Review Letters*, 1993, **70**, 1557–1560.
- 13 R. Pesché, M. Kollmann and G. Nägele, *The Journal of Chemical Physics*, 2001, **114**, 8701.
- 14 M. McPhie and G. Nägele, *The Journal of chemical physics*, 2007, **127**, 034906.
- 15 V. Kalikmanov, *Nucleation Theory*, 2013, 17–41.
- 16 M. Radu and T. Schilling, *EPL (Europhysics Letters)*, 2014, **105**, 26001.
- 17 B. Dünweg and A. J. C. Ladd, *Advanced Computer Simulation Approaches for Soft Matter Sciences III*, Springer-Verlag Berlin, Berlin, Germany, 2009, vol. 221, pp. 89–166.
- 18 H. Andersen, *The Journal of Chemical Physics*, 1980, **72**, 2384.
- 19 E. Meijer and D. Frenkel, *The Journal of chemical physics*, 1991, **94**, 2269.
- 20 S. Hamaguchi, R. Farouki and D. Dubin, *Physical Review E*, 1997, **56**, 4671.
- 21 J. D. Weeks, D. Chandler and H. C. Andersen, *Journal of Chemical Physics*, 1971, **54**, 5237.
- 22 R. Adhikari, K. Stratford, M. Cates and A. Wagner, *Europhysics Letters*, 2005, **71**, 473.
- 23 U. D. Schiller, *PhD thesis*, Johannes Gutenberg-Universität Mainz, Fachbereich 08: Physik, Mathematik und Informatik, 2008.
- 24 P. Ahlrichs and B. Dünweg, *Journal of Chemical Physics*, 1999, **111**, 8225–8239.
- 25 D. P. Ziegler, *Journal of Statistical Physics*, 1993, **71**, 1171–1177.
- 26 P. J. Hoogerbrugge and J. M. V. A. Koelman, *Europhysics Letters*, 1992, **19**, 155–160.
- 27 P. Español and P. Warren, *Europhysics Letters*, 1995, **30**, 191.
- 28 O. B. Usta, A. J. C. Ladd and J. E. Butler, *Journal of Chemical Physics*, 2005, **122**, 094902.
- 29 D. Frenkel, *Science*, 2002, **296**, 65.
- 30 H. J. Limbach, A. Arnold, B. A. Mann and C. Holm, *Comp. Phys. Comm.*, 2006, **174**, 704–727.
- 31 A. Arnold, O. Lenz, S. Kesselheim, R. Weeber, F. Fahrenberger, D. Röhm, P. Košovan and C. Holm, *Meshfree Methods for Partial Differential Equations VI*, 2013, pp. 1–23.
- 32 D. Roehm and A. Arnold, *EPJ -ST*, 2012, **210**, 89–100.
- 33 P. Steinhardt, D. Nelson and M. Ronchetti, *Physical Review B*, 1983, **28**, 784.
- 34 D. Moroni, P. Ten Wolde and P. Bolhuis, *Physical Review Letters*, 2005, **94**, 235703.
- 35 W. Lechner and C. Dellago, *The Journal of chemical physics*, 2008, **129**, 114707.